10-25-2022

Discovery of a novel genomic alteration that renders leukemic cells resistant to CD19-targeted immunotherapies

Armin Ghobadi

Jack H Landmann

Alun Carter

Matthew L Cooper

Mehmet Emrah Selli

See next page for additional authors

Authors

Armin Ghobadi, Jack H Landmann, Alun Carter, Matthew L Cooper, Mehmet Emrah Selli, Jufang Chang, Christopher A Miller, Francesca Ferraro, David Y Chen, Amanda M Smith, Taylor A LaValle, Eric J Duncavage, Nathan Singh, and et al.

RESEARCH LETTER

blood advances

TO THE EDITOR:

Discovery of a novel genomic alteration that renders leukemic cells resistant to CD19-targeted immunotherapies

Armin Ghobadi,[1] Jack H. Landmann,[1] Alun Carter,[1] Matthew L. Cooper,[1] Mehmet Emrah Selli,[1] Jufang Chang,[1] Matthew Baker,[2,3] Christopher A. Miller,[1] Francesca Ferraro,[1] David Y. Chen,[1] Amanda M. Smith,[1] Taylor A. LaValle,[1] Eric J. Duncavage,[1] Justin Chou,[4] Victor Tam,[4] Joseph M. Benoun,[4] Jenny Nater,[4] Nathalie Scholler,[4] Francesca Milletti,[4] Remus Vezan,[4] Adrian Bot,[4] John M. Rossi,[4] and Nathan Singh[1]

[1]Division of Oncology, Washington University School of Medicine, St. Louis, MO; [2]The University of Texas Health Science Center at Houston, Houston, TX; [3]Department of Biochemistry and Molecular Biology, Baylor College of Medicine, Houston, TX; and [4]Kite, a Gilead Company, Santa Monica, CA

CD19-targeted immunotherapies that stimulate a cytotoxic T-cell response have revolutionized the management of B-cell malignancies, specifically relapsed or refractory acute lymphoblastic leukemia (R/R ALL). Blinatumomab is an anti-CD19 bispecific T-cell engager approved for the treatment of patients with R/R ALL.[1] KTE-X19 is an autologous anti-CD19 chimeric antigen receptor (CAR) T-cell therapy under investigation in the ZUMA-3 (XXX) phase 1/2 clinical trial (registered at www.clinicaltrials.gov as #NCT02614066) for adult patients with R/R ALL.[2] The emergence of leukemic clones that have lost surface expression of CD19 is a cause of disease relapse in 10% to 25% of patients treated with either blinatumomab or CAR T cells.[1-5] Several distinct mechanisms have been documented, including truncating mutations in the transmembrane domain of CD19 that prevent surface expression,[5] as well as alternative messenger RNA splicing that results in loss of the antigenic epitope and prevents CAR binding.[3,4] Here we describe the discovery of a novel genomic modification outside of the transmembrane and antigenic domains of CD19 that enable resistance to blinatumomab and KTE-X19.

A 60-year-old woman with B-cell ALL was treated with chemotherapy followed by 2 cycles of blinatumomab as initial therapy. She experienced disease relapse after the second cycle of blinatumomab and was enrolled in the ZUMA-3 investigational study of KTE-X19. She received a single infusion of anti-CD19 CAR T cells at the target dose but had no disease response.

Pathologic evaluation performed at her local hospital before enrollment in ZUMA-3 characterized a homogenous population of $CD19^{dim}$ lymphoblasts (evaluated by flow cytometry using anti-CD19 antibody clone J3-119). Evaluation of postblinatumomab relapse lymphoblasts at our tertiary care center using FMC63, the parental anti-CD19 antibody clone used to derive KTE-X19, demonstrated $CD19^{-}$ disease (Figure 1A; supplemental Figure 1A). Using targeted RNA sequencing of ALL cells collected after KTE-X19 failure, we detected an in-frame deletion of the nucleotides encoding tyrosine 260 within exon 4 of CD19 in relapsed leukemic cells. Notably, predictive modeling[6] did not suggest significant disruption of the CD19 extracellular structure or the FMC63 binding site as result of this deletion (Figure 1B).

We performed sequential exome and RNA sequencing on leukemic cells from diagnosis and relapse (postblinatumomab) and after KTE-X19 to trace the clonal evolution of this leukemia (supplemental Table 1). We determined that the founding clone (present at diagnosis and all subsequent samples) had loss of heterozygosity for CD19 as a result of a whole-chromosome loss of chromosome 16 (as well as loss of chromosomes 2, 3, 7, 12, 13, 15, 17, and 20). In addition, we identified a subclone within the diagnostic sample that was not present in the postblinatumomab sample (Figure 1C). In the postblinatumomab sample, we detected the emergence of a subclone that harbored a deletion of the

Submitted 31 March 2022; accepted 28 June 2022; prepublished online on *Blood Advances* First Edition 20 July 2022; final version published online xxx. https://doi.org/10.1182/bloodadvances.2022007705.

Reagents and data from this manuscript are available from the corresponding author upon request: nathan.singh@wustl.edu. The complete data set, including reads for all DNA and RNA sequencing experiments, is available through the Database of Genotypes and Phenotypes at accession ID phs002721.v1.p1.

The full-text version of this article contains a data supplement.

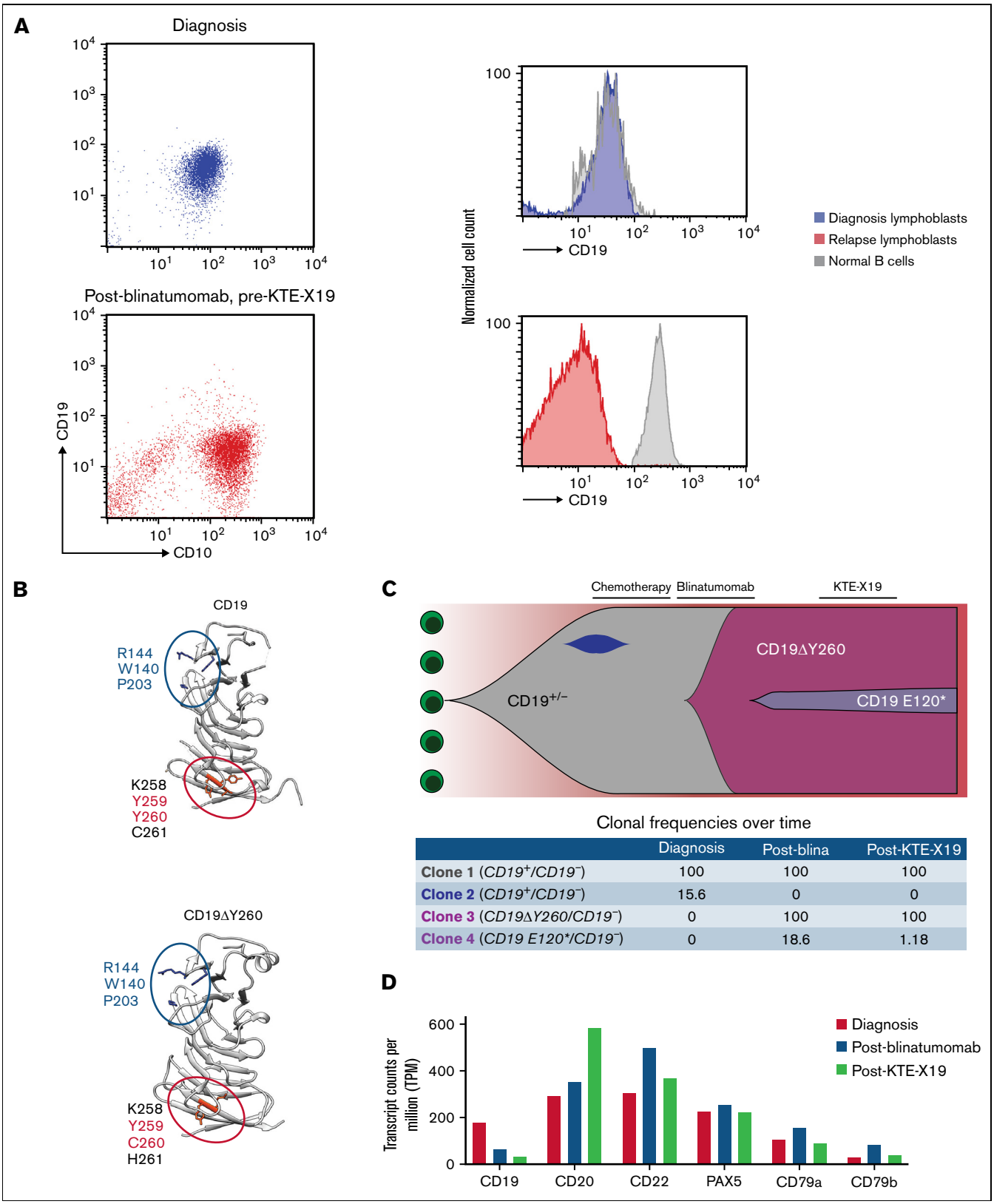

	Diagnosis	Post-blina	Post-KTE-X19
Clone 1 (*CD19⁺/CD19⁻*)	100	100	100
Clone 2 (*CD19⁺/CD19⁻*)	15.6	0	0
Clone 3 (*CD19ΔY260/CD19⁻*)	0	100	100
Clone 4 (*CD19 E120*/CD19⁻*)	0	18.6	1.18

Figure 1. Emergence of a leukemic clone with a deletion of Tyr260 in CD19. (A) Diagnostic flow cytometry demonstrates loss of surface CD19 during treatment with CD19-targeted immunotherapies. Scatter plots of pretreatment (bone marrow) and postblinatumomab (peripheral blood) lymphoblasts stained with the anti-CD19 antibody FMC63 and costained with antibodies against CD10 (left). Histograms of CD19 and CD10 expression by lymphoblasts and other hematopoietic cells pre- and postblinatumomab treatment (right). (B) Predictive protein structural modeling of wild-type (WT) and ΔY260 CD19. Residues essential for FMC63 binding are shown in

codon encoding Y260 (CD19ΔY260), which was also present in the sample collected after failure of CAR T-cell therapy (Figure 1C). The allelic frequency of CD19ΔY260 following blinatumomab was 90.47% and 82.75% of total B cells (malignant and contaminating normal B cells) following KTE-X19, reflecting a high clonal burden at both times of therapeutic failure. Droplet digital polymerase chain reaction (ddPCR) confirmed that this deletion was not present in leukemic blasts at time of diagnosis. In addition to this deletion, we detected a truncating mutation within the *CD19* coding region (E120*) with low variant allele frequency (Figure 1C), suggesting that it did not substantively contribute to therapeutic failure. We confirmed that the observed enrichment of CD19ΔY260 was the result of a clonal expansion by tracing cooccurring somatic mutations, which demonstrated clustering of these mutations with CD19ΔY260 over time (supplemental Figure 1B).

We quantified specific genes and pathways that we hypothesized to be involved in regulating response to CD19-directed immunotherapy. We observed a decrease in CD19 transcript counts after blinatumomab, whereas expression of other B cell lineage–defining genes remained stable or increased (Figure 1D), confirming B lineage commitment of this leukemia. Consistent with previous studies evaluating changes in gene expression after immunotherapeutic pressure,[7-9] expression of major histocompatibility complex class II genes decreased after blinatumomab and CAR T-cell therapy. Further evaluation revealed suppression of B-cell receptor signaling but did not reveal consistent alterations in non–B-cell receptor pathways (supplemental Figure 1C).

To confirm that loss of Y260 was mechanistically responsible for resistance to CD19-directed therapy, we synthesized WT and ΔY260 transgenes (supplemental Figure 2A) and expressed these in Jurkat cells, an immortalized T lymphoid cell line that endogenously lacks CD19 expression. The plasmids encoding these transgenic CD19 sequences also contained a green fluorescent protein (GFP) reporter to enable facile identification of engineered cells (supplemental Figure 2B). Engineered Jurkats were combined with primary human T cells expressing a CD19-targeted CAR. Evaluation of these cocultures using flow cytometry revealed that expression of CD19ΔY260 enabled marked resistance to CAR T-cell cytotoxicity (Figure 2A). To confirm this resistance using a distinct system, we combined GFP^- Jurkat (nonengineered, $CD19^-$) cells with GFP^+ Jurkats (expressing either CD19 or CD19ΔY260) at a 1:1 ratio and also combined these mixed populations with CD19-targeted CAR T cells. Evaluation of these cultures again demonstrated that cells expressing CD19ΔY260 were resistant to CAR killing, as reflected by maintenance of the 1:1 ratio of engineered to nonengineered Jurkats (Figure 2B).

Diagnostic flow cytometry demonstrated that the anti-CD19 antibody FMC63 failed to bind CD19ΔY260 on the surface of the relapsed leukemia (Figure 1A). We confirmed that additional antibody clones also did not bind CD19ΔY260 (Figure 2C-D). We hypothesized that this failed binding could have occurred as a result of either (1) alteration of the antibody binding epitopes or (2) failed surface expression of CD19. To evaluate this, we generated CD19 genes (WT or ΔY260) with an N-terminal FLAG tag, segregating anti-CD19 antibody binding from surface expression. These transgenic constructs also encoded a truncated CD34 expression marker to enable confirmation of genetic engineering (supplemental Figure 2C). Extracellular staining for surface protein expression demonstrated that cells engineered with FLAG-CD19 (WT) costained for FLAG and CD19, whereas cells engineered with FLAG-CD19ΔY260 stained for neither (Figure 2E), indicating that loss of Y260 prevents surface expression of CD19. Given the lack of surface expression, these studies were unable to evaluate if loss of Y260 affected anti-CD19 antibody binding. To determine this, we performed intracellular staining for FLAG and CD19 (using FMC63) and found that loss of Y260 had no impact on binding of the FLAG antibody, confirming protein expression. Intriguingly, ΔY260 significantly reduced but did not completely abrogate FMC63 binding to CD19 (Figure 2F). Together, these data indicate that loss of Y260 leads to failed surface presentation of CD19 as well as alteration of the FMC63 binding site.

In order to identify the etiology of this failed surface expression, we performed fractionated cell lysate electrophoresis to determine where this intracellular retention occurred. Immunoblotting for CD19 revealed that CD19ΔY260 was found in both cytosolic and membrane compartments and concurrently demonstrated that CD19ΔY260 migrated at a lower molecular weight than WT CD19 (Figure 2G). CD19 undergoes extensive posttranslational *N*-glycosylation as it transits through the Golgi en route to the cell surface, which results in the production of CD19 proteins that run at several molecular weights.[10] This glycosylation was recently shown to be required for surface expression of CD19.[11] To confirm that the reduction in molecular weight seen for CD19ΔY260 was a result of hypoglycosylation, we treated lysates from cells expressing either WT or ΔY260 CD19 with peptide:*N*-glycosidase F to cleave all *N*-linked glycans. We found this reduced the molecular weight of WT CD19 to that of CD19ΔY260 (Figure 2H), confirming CD19ΔY260 was hypoglycosylated. These data indicate that CD19ΔY260 is not expressed on the cell surface but localizes to membrane structures, binds FMC63 with less efficiency, and is hypoglycosylated, which collectively strongly suggest that loss of Y260 leads to antigen escape by promoting retention of CD19 within the Golgi.

Using sequential exome and genome sequencing, we identified the emergence of an ALL clone with a deletion of Y260 in *CD19*. In vitro modeling confirmed that this alteration to CD19 led to reduced antibody binding, failed posttranslational modification, disrupted surface presentation, and failure of CAR T-cell therapy. Antigen escape has emerged as the most common tumor-intrinsic etiology of immunotherapy failure.[12] Previous work has demonstrated that loss of large gene fragments (such as all of exon 2) can lead to antigen escape by altering protein structure and leading to Golgi retention.[4,5] We demonstrate that loss of a single amino acid can alter protein processing and enable antigen escape, underscoring that minor changes in antigen biology can have a significant impact on immunotherapeutic efficacy. Although we

Figure 1 (continued) blue, and residues surrounding Tyr260 are shown in orange. (C) Schematic representation of inferred evolutionary trajectory of CD19ΔY260. Dark blue ellipse represents a clone that was detectable at diagnosis but disappeared after initial chemotherapy. Table below reflects allele frequency of each clone over time normalized to percentage of cells collected that were malignant (~90% for clone 3 across time points). (D) Quantification of B-cell lineage transcripts in diagnosis, postblinatumomab, and post–CAR T-cell treatment ALL cells.

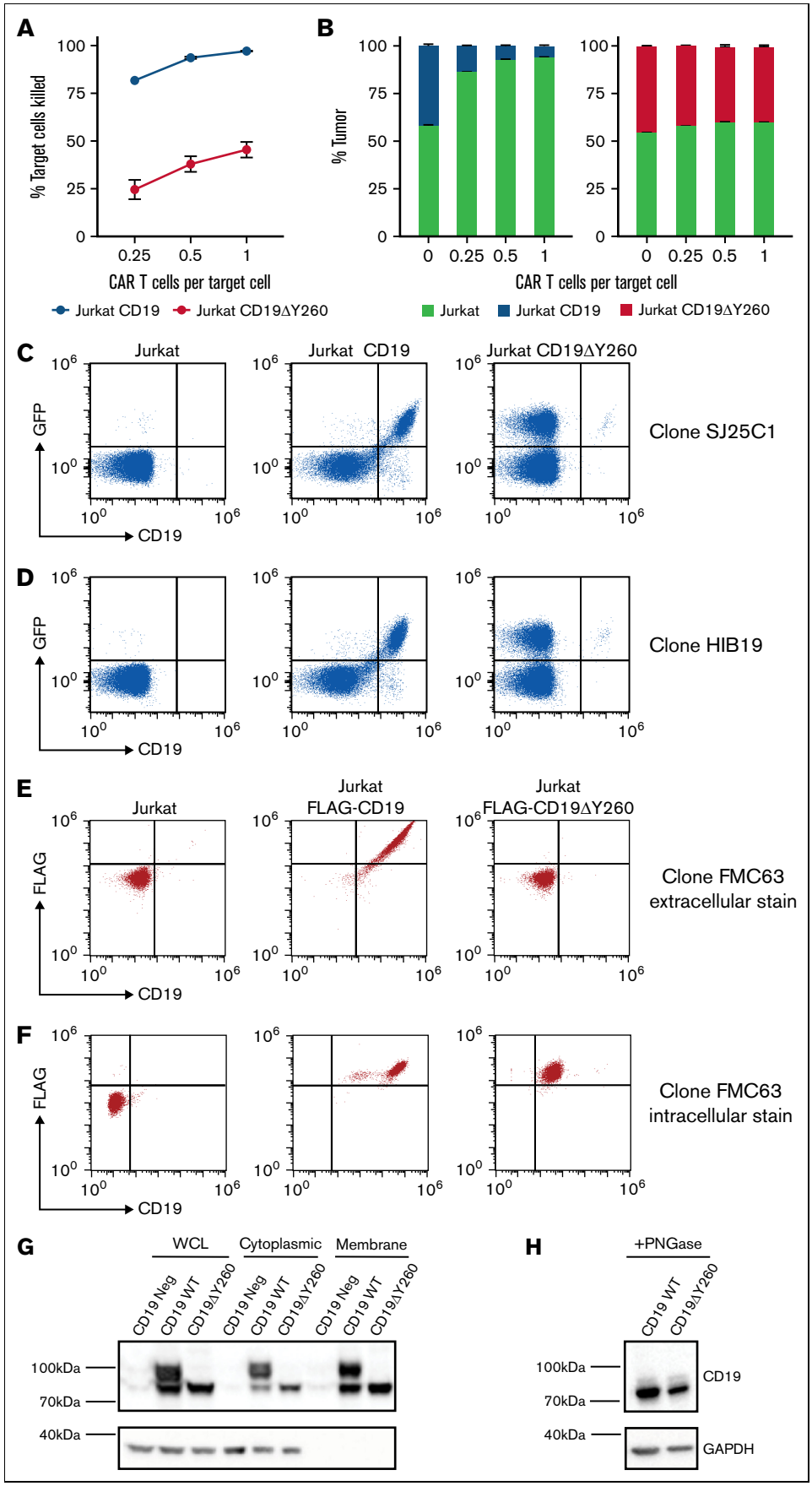

Figure 2.

have not confirmed the etiology of retention within the Golgi, we speculate that loss of Y260 does indeed affect overall protein structure, which leads to failed organellar transit. These findings compel detailed correlative studies in other instances of antigen escape to identify if loss of Y260 is a recurrent cause of failure, as well as to identify other alterations that can cause antigen escape.

Peripheral blood mononuclear cells were collected from a patient with B-cell ALL at diagnosis, before CAR T-cell therapy (post-blinatumomab/pre–KTE-X19 therapy), and post–KTE-X19 infusion (30 days postinfusion). Therapies before KTE-X19 included induction chemotherapy, followed by blinatumomab and then hyperCVAD (hyperfractionated cyclophosphamide, vincristine, doxorubicin, and dexamethasone). Bone marrow samples were collected at diagnosis, postblinatumomab/pre–KTE-X19 therapy, and post–KTE-X19 therapy. Lymphoblasts were gated as side scatter low, CD45 low cells. Normal B cells were identified by gating remaining cells for high expression of CD19.

Enhanced whole-exome (with added exome capture, IDT exome reagent, target coverage 200×) and whole-transcriptome (target coverage 60× for tumor and 30× for matched control) sequencing were performed as previously described.[13] The full pipeline with all parameters is described in a Common Workflow Language pipeline (https://git.io/JRFnM). Briefly, reads were aligned to the reference sequence build GRCh38 using BWA-MEM (version 0.7.15; https://arxiv.org/abs/1303.3997). Somatic variants were called using 4 tools (GATK,[14] Mutect2 [version 4.1.2.0],[15] Strelka [version 2.9.9],[16] Varscan [version 2.4.2],[17] and Pindel [version 0.2.5b8][18]) and then filtered, merged, and annotated with the Ensembl Variant Effect Predictor.[19] Copy-number changes between tumor and matched normal samples were defined with copycat (https://github.com/chrisamiller/copyCat). Clonal clustering was performed with the sciClone algorithm.[20] The complete data set, including reads for all DNA and RNA sequencing experiments, is available through dbGaP at accession ID phs002721.v1.p1.

All ddPCR reagents were from Bio-Rad. CD19 and CD19ΔY260 primers and probes for ddPCR were designed using the Bio-Rad Web site as per Minimum Information for Publication of Quantitative Real-Time PCR Experiments guidelines.[21] Droplet generation was achieved using the Bio-Rad QX100 and QX200 Droplet Digital PCR Systems, and ddPCR was performed and analyzed as previously described.[22] The optimal annealing temperature for this assay, defined as the temperature that allowed for optimal droplet separation, was determined by temperature gradient to be 53.6°C. The sensitivity of this assay was determined through serial dilution of positive control DNA into WT DNA and calculated to be 1:100 000. In each well, 200 ng of patient DNA were tested for Tyr260 deletion (for a total of 1 μg of DNA across 5 wells) per tested sample. DNA was digested with *Hin*dIII at 1 μL per well to ensure maximum DNA accessibility. The data were visualized and analyzed using Bio-Rad Quanta Software (QuantaSoft AP software).

Models for CD19 were generated using the PDB template 6AL5. Both WT and CD19ΔY260 were modeled using Phyre2 software.[6] Visualization, analysis, and comparison of the models were performed using UCSF Chimera. Identification of the FMC63 binding epitope was based on previously published data.[10]

Cells were maintained in a tissue culture incubator at 37°C 5% CO_2 unless stated otherwise. Jurkat and Raji tumor cells were cultured in RPMI 1640 (Corning) supplemented with 10% heat-inactivated fetal bovine serum (FBS), 1% GlutaMAX (Life Technologies), and 1% penicillin/streptomycin (pen/strep; Thermo Fisher Scientific). Dulbecco's modified eagle medium (Thermo Fisher Scientific) with 10% FBS, 1% GlutaMAX, and pen/strep was used for 293T culture. T cells/CAR T cells were cultured in RPMI 1640 with 10% FBS, 1% GlutaMAX, 1% pen/strep, 5×10^{-5} M of β-mercaptoethanol, 20 mM of HEPES, 50 U/mL of interleukin-2 (IL-2; Peprotech), 10 ng/mL of IL-15 (Peprotech), and 10 ng/mL of IL-7 (Peprotech). Where stated, cells were washed in phosphate-buffered saline (PBS; pH, 7.5; Corning) or fluorescence-activated cell-sorting (FACS) buffer (PBS supplemented with 2 mM of EDTA; Sigma-Aldrich) and 0.5% bovine serum albumin (Sigma-Aldrich).

Transgenic CD19 vectors were commercially generated (Vectorbuilder, Inc., Chicago, IL). CD19 (NM_001178098) internal ribosome entry site–enhanced GFP protein was synthesized and cloned into a pLVM-EF1a lentiviral vector. For the delY260 construct, CD19 (NM_001178098) internal ribosome entry site–enhanced GFP was modified to remove the codon encoding Tyr260, synthesized and cloned into the same parental pLVM-EF1a lentiviral backbone. For FLAG-tagged CD19 studies, the CD19 signal peptide was replaced by the murine β_2-microglobulin signal peptide, followed by FLAG sequence.

Lentiviral particles were generated as previously described.[23] Jurkat (ATCC TIB-152) cells were transduced with CD19-encoding lentiviral vectors at a multiplicity of infection of 1. Jurkat cells engineered with GFP-containing constructs subsequently underwent FACS using GFP on the Synergy HAPS (Sony) to achieve purity >98%. For CD19-specific CAR T-cell (CART19) production (19-28ζ), human T cells were purified from peripheral blood mononuclear cells using $CD4^+$ and $CD8^+$ selection according to manufacturer instructions (Miltenyi) and activated with CD3/CD28 (Dynabeads). T cells were transduced with CART19s at +24 hours, and stimulation was removed at +48 hours. CART19s were harvested on day 11, and transduction efficiency was confirmed using flow cytometry, followed by purification for CAR^+ cells using FACS.

Figure 2. Loss of Tyr260 results in resistance to CAR T cells by preventing surface expression of CD19. (A) Percentage of Jurkat cells engineered to express either WT or CD19ΔY260 that were killed by CAR T cells. Cocultures were established at several effector-to-target ratios, and measurements were taken after 48 hours. (B) Jurkat cells engineered to express either WT or ΔY260 with a GFP marker were combined with nonengineered $CD19^-$ GFP^- Jurkats at a ratio of 1:1, and these mixed cell pools were combined with CD19 CAR T cells. Data represent composition of cocultures after 48 hours. (C-D) Jurkat cells were engineered to express either WT or ΔY260 CD19 with a GFP marker, and binding of anti-CD19 antibodies SJ25C1 (C) and HIB19 (D) was evaluated by flow cytometry. (E-F) Jurkat cells were engineered to express either WT or ΔY260 CD19 that was linked to an N-terminal FLAG tag, and expression of CD19 and FLAG was determined by extracellular staining (E) or intracellular staining (F) and analysis by flow cytometry. (G) Jurkat cells engineered with nothing ($CD19^-$), WT, or ΔY260 CD19 underwent fractionated cellular lysis. Lysates from the whole cell (WCL) or cytoplasmic or membrane compartments were separated by electrophoresis, and membranes were stained for CD19 or glyceraldehyde-3-phosphate dehydrogenase (GAPDH; loading control). (H) Peptide:*N*-glycosidase (PNGase) F–treated whole-cell lysates from Jurkats expressing either WT or ΔY260 CD19 were probed for CD19 or GAPDH (loading control).

To prepare cell lysates, 5×10^6 tumor cells were washed with PBS and placed on ice during processing. Cell protein fractionation was performed using a cell fractionation kit (Cell Signaling Technology) according to manufacturer protocols. For cell lysate deglycosylation, cell pellets were resuspended in 240 μL of NPER (Bio-Rad) lysis buffer, 30 μL of Deglycosylation Mix Buffer II (New England Biolabs), and Halt Protease inhibitor cocktail (Thermo Fisher Scientific) according to manufacturer protocols. Samples were incubated at 100°C for 10 minutes, sonicated 3 times for 10 seconds at 50% amplitude, and separated into 2 aliquots. Fifteen microliters of Deglycosylation Enzyme Mix II (New England Biolabs) or PBS was added to the replicate processed cell lysates, which were then incubated at 37°C for 16 hours before western blot analysis. NuPAGE LDS sample buffer (Thermo Fisher Scientific) and western blotting were performed using standard protocols. In brief, after electrophoresis, membranes were blocked using 5% milk and subsequently stained with primary antibody mouse anti-human CD19 clone LE-CD19 (1:2000; Novus Biological) or rabbit anti-human glyceraldehyde-3-phosphate dehydrogenase clone D16H11 (1:2000; Cell Signaling Technologies). Membranes were washed and stained with horseradish peroxidase–conjugated anti-mouse (1:5000) or anti-rabbit (1:2000) secondary antibodies. Blots were washed and developed with Luminata Crescendo ELC reagent (EMD Millipore) according to manufacturer protocols and were imaged using the ChemiDoc imager system (Bio-Rad). Western blot analysis was performed in duplicate.

For CART19 killing assays, nontransduced, WT, and delY260-transduced Jurkat cells were stained with CellTrace Violet (Invitrogen) according to manufacturer protocols and subsequently cultured for an additional 24 hours in RPMI at 37°C before assay. Killing assays were performed in RPMI (10% FBS, 1% GlutMAX, and pen/strep), and tumor cells were seeded in a 96-well plate at a total of 25 000 cells per well. For specified killing assays, non-transduced Jurkat cells were plated at a 1:1 ratio with CD19 or delY260 before addition of CART19s. CART19s were serially diluted and added to tumor cells at effector-to-target ratios of 1:4, 1:2, and 1:1. After 48 hours of incubation at 37°C, tumor killing was analyzed by flow cytometry as described in the next paragraph. Data replicates were $n = 4$, and statistical analyses were performed in GraphPad Prism 8 using 2-way analysis of variance.

Cocultures were washed and resuspended in FACS buffer for cell staining. For staining, 7-AAD solution (BD Biosciences) was included in all stains at 1:40. Antibodies used were phycoerythrin mouse anti-human CD34 pool kit (1:50; Beckman Coulter), APC mouse anti-human CD19 clone HIB19 (1:50; BD Biosciences), APC mouse anti-human CD19 clone SJ25-C1 (1:20; BD Biosciences), and BV650 mouse anti-human CD3 clone UCHT1 (1:50; BD Biosciences). Before analysis, stained cells were washed in FACS buffer and analyzed using the Attune NxT flow cytometer (Thermo Fisher Scientific). For surface FLAG/CD19 analysis, Jurkat cells were washed as described and stained with anti-FLAG (A01632; BD Biosciences) and anti-CD19 (FMC63; FM3-BY45; Acro Biosystems) antibodies and analyzed as described.

Acknowledgments: The authors thank the patient, patient's family, and caregivers, as well as the study staff at each site. The authors also thank Daved Fremont (Washington University Department of Biochemistry) for guidance with CD19 surface expression studies.

Medical writing support was provided by Nexus Global Group Science, funded by Kite, a Gilead Company.

Contribution: A.G., M.L.C., C.A.M., A.B., J.M.R., and N. Singh formulated the ideas and planned the experiments; J. Chang and M.B. performed in silico analyses; C.A.M. performed DNA and RNA sequencing and analyzed the sequencing data; F.F. performed ddPCR; J.H.L., M.E.S., A.C., D.Y.C., A.M.S., T.A.L.V., and N. Singh performed and analyzed in vitro experiments; E.J.D. and J. Chou reviewed diagnostic flow cytometry data; V.T., J.M.B., J.N., N. Scholler, F.M., and R.V. provided intellectual support; A.G., M.L.C., M.B., C.A.M., F.F., and N. Singh wrote the manuscript; and all authors reviewed and edited the manuscript.

Conflict-of-interest disclosure: A.G. declares a consulting or advisory role for Kite, a Gilead Company, Amgen, Atara, Wugen, and Celgene; research funding from Kite and Amgen; and honoraria from Kite. M.L.C. is employed by and has stock or other ownership in Wugen; reports a consultancy or advisory role for Rivervest Ventures; and reports patents, royalties, or other intellectual property from Wugen and NeoImmuneTech. F.F. has patents and receives royalties from Magenta (unrelated to this work). A.C. is employed by and has stock or other ownership in Wugen. J. Chou, F.M., and A.B. are employed by Kite. V.T., J.M.B., R.V., and J.M.R. were formerly employed by Kite. J.M.B. has stock or other ownership in Gilead Sciences, Allogene, Aurinia Pharma, and TG Therapeutics. J.N. has stock or other ownership in Kite. N. Scholler is employed by Gilead; was formerly employed by with Kite; and reports stock or other ownership in Gilead Sciences, Bristol-Myers Squibb, and Seattle Genetics. N. Singh has several patents related to CAR T cells and other cellular immunotherapies. The remaining authors declare no competing financial interests.

ORCID profiles: A.G., 0000-0001-8848-8474; M.E.S., 0000-0002-3478-8970; M.B., 0000-0001-9039-8523; C.A.M., 0000-0003-4266-6700; D.Y.C., 0000-0002-3681-6576; A.M.S., 0000-0002-8716-6745; J.N., 0000-0001-9495-0653.

Correspondence: Armin Ghobadi, Center for Gene and Cellular Immunotherapy, Washington University School of Medicine, Division of Medical Oncology, Section of Stem Cell Transplant and Leukemia, 660 S. Euclid Ave, Campus Box 8007-29, St. Louis, MO 63110; email: arminghobadi@wustl.edu; and Nathan Singh, Washington University School of Medicine, Division of Oncology, 660 S. Euclid Ave, St. Louis, MO 63110; email: nathan.singh@wustl.edu.

References

1. Topp MS, Gökbuget N, Zugmaier G, et al. Phase II trial of the anti-CD19 bispecific T cell-engager blinatumomab shows hematologic and molecular remissions in patients with relapsed or refractory B-precursor acute lymphoblastic leukemia. *J Clin Oncol*. 2014;32(36):4134-4140.
2. Shah BD, Ghobadi A, Oluwole OO, et al. KTE-X19 for relapsed or refractory adult B-cell acute lymphoblastic leukaemia: phase 2 results of the single-arm, open-label, multicentre ZUMA-3 study. *Lancet*. 2021;398(10299):491-502.
3. Bagashev A, Sotillo E, Tang CH, et al. CD19 alterations emerging after CD19-directed immunotherapy cause retention of the misfolded

protein in the endoplasmic reticulum. *Mol Cell Biol*. 2018;38(21): e00383-18.

4. Sotillo E, Barrett DM, Black KL, et al. Convergence of acquired mutations and alternative splicing of CD19 enables resistance to CART-19 immunotherapy. *Cancer Discov*. 2015;5(12):1282-1295.
5. Orlando EJ, Han X, Tribouley C, et al. Genetic mechanisms of target antigen loss in CAR19 therapy of acute lymphoblastic leukemia. *Nat Med*. 2018;24(10):1504-1506.
6. Kelley LA, Mezulis S, Yates CM, Wass MN, Sternberg MJ. The Phyre2 web portal for protein modeling, prediction and analysis. *Nat Protoc*. 2015;10(6):845-858.
7. Christopher MJ, Petti AA, Rettig MP, et al. Immune escape of relapsed AML cells after allogeneic transplantation. *N Engl J Med*. 2018; 379(24):2330-2341.
8. Chen PH, Lipschitz M, Weirather JL, et al. Activation of CAR and non-CAR T cells within the tumor microenvironment following CAR T cell therapy. *JCI Insight*. 2020;5(12):134612.
9. Axelrod ML, Cook RS, Johnson DB, Balko JM. Biological consequences of MHC-II expression by tumor cells in cancer. *Clin Cancer Res*. 2019;25(8):2392-2402.
10. Klesmith JR, Wu L, Lobb RR, Rennert PD, Hackel BJ. Fine epitope mapping of the CD19 extracellular domain promotes design. *Biochemistry*. 2019;58(48):4869-4881.
11. Mortales CL, Lee SU, Demetriou M. *N*-glycan branching is required for development of mature B cells. *J Immunol*. 2020;205(3):630-636.
12. Singh N, Orlando E, Xu J, et al. Mechanisms of resistance to CAR T cell therapies. *Semin Cancer Biol*. 2020;65:91-98.
13. Miller CA, Dahiya S, Li T, et al. Resistance-promoting effects of ependymoma treatment revealed through genomic analysis of multiple recurrences in a single patient. *Cold Spring Harb Mol Case Stud*. 2018;4(2):a002444.
14. McKenna A, Hanna M, Banks E, et al. The Genome Analysis Toolkit: a MapReduce framework for analyzing next-generation DNA sequencing data. *Genome Res*. 2010;20(9): 1297-1303.
15. Cibulskis K, Lawrence MS, Carter SL, et al. Sensitive detection of somatic point mutations in impure and heterogeneous cancer samples. *Nat Biotechnol*. 2013;31(3):213-219.
16. Kim S, Scheffler K, Halpern AL, et al. Strelka2: fast and accurate calling of germline and somatic variants. *Nat Methods*. 2018;15(8): 591-594.
17. Koboldt DC, Zhang Q, Larson DE, et al. VarScan 2: somatic mutation and copy number alteration discovery in cancer by exome sequencing. *Genome Res*. 2012;22(3):568-576.
18. Ye K, Schulz MH, Long Q, Apweiler R, Ning Z. Pindel: a pattern growth approach to detect break points of large deletions and medium sized insertions from paired-end short reads. *Bioinformatics*. 2009;25(21):2865-2871.
19. McLaren W, Gil L, Hunt SE, et al. The Ensembl Variant Effect Predictor. *Genome Biol*. 2016;17(1):122.
20. Miller CA, White BS, Dees ND, et al. SciClone: inferring clonal architecture and tracking the spatial and temporal patterns of tumor evolution. *PLOS Comput Biol*. 2014;10(8):e1003665.
21. Bustin SA, Benes V, Garson JA, et al. The MIQE guidelines: minimum information for publication of quantitative real-time PCR experiments. *Clin Chem*. 2009;55(4):611-622.
22. Hindson BJ, Ness KD, Masquelier DA, et al. High-throughput droplet digital PCR system for absolute quantitation of DNA copy number. *Anal Chem*. 2011;83(22):8604-8610.
23. Cooper ML, Choi J, Staser K, et al. An "off-the-shelf" fratricide-resistant CAR-T for the treatment of T cell hematologic malignancies. *Leukemia*. 2018;32(9):1970-1983.